Dalton Transactions

Hydrothermal Synthesis and Structural Characterization of Several Complex Rare Earth Tantalates: Ln2TaO5(OH) (Ln = La, Pr) and Ln3Ta2O9(OH) (Ln = Pr, Nd)

Journal:	*Dalton Transactions*
Manuscript ID	DT-ART-01-2019-000059.R1
Article Type:	Paper
Date Submitted by the Author:	08-Feb-2019
Complete List of Authors:	Sanjeewa, Liurukara; Oak Ridge National Laboratory, Material Sciences; Clemson University College of Engineering and Sciences, Fulle, Kyle; Clemson University, Department of Chemistry McMillen, Colin; Clemson University, Department of Chemistry Kolis, Joseph; Clemson University

Hydrothermal Synthesis and Structural Characterization of Several Complex Rare Earth Tantalates: $Ln_2TaO_5(OH)$ (*Ln* = La, Pr) and $Ln_3Ta_2O_9(OH)$ (*Ln* = Pr, Nd)

Liurukara D. Sanjeewa, Kyle Fulle, Colin D. McMillen, Joseph W. Kolis*

Department of Chemistry and Center for Optical Materials Science and Engineering Technologies (COMSET), Clemson University, Clemson, South Carolina 29634-0973, USA

Abstract

Reactions are reported of early rare earth oxides, RE_2O_3 (*RE* = La, Pr, Nd) with Ta_2O_5 under hydrothermal conditions (650˚C, 1.5kbar) in concentrated aqueous hydroxide (20-30 M KOH) as a mineralizer. Under various stoichiometries several members of two new structure types were isolated, $Ln_2TaO_5(OH)$ (*Ln* = La, Pr) and $Ln_3Ta_2O_9(OH)$ (*Ln* = Pr, Nd). The analogous niobate $La_2NbO_5(OH)$ was also obtained. Both structure types were characterized by single crystal x-ray diffraction and contain pentavalent tantalatum oxide octahedra and complex rare earth oxide frameworks. The $Ln_2TaO_5(OH)$ structure type contains Ln-O_8 and Ln-O_9 building blocks and TaO_6 octahedra in a 3-D framework. It contains a 3-D rare earth oxide framework formed by from zig-zag chains of rare earth oxides linking sheets of rare earth oxides. The tantalates form edge-shared Ta_2O_{10} dimers occupying gaps in the rare earth oxide frameworks. The structure of $Ln_3Ta_2O_9(OH)$ contains two types of 2-D rare earth oxide slabs built of seven and eight coordinate rare earth metals. The tantalate units form 2-D slabs through a multiple corner-sharing scheme of TaO_6 octahedra. The $Ln_3Ta_2O_9(OH)$ structure type has an interesting close structural relationship to the previously reported rare earth titanate $La_5Ti_4O_{15}(OH)$, which is discussed. The presence of hydroxide in the lattice is confirmed by IR spectroscopy and the H atom locations are assigned unambiguously using bond valence sums.

1. INTRODUCTION

The structural and reaction chemistry of refractory oxides is an important area of current research activity, and they find use as catalysts, oxide conductors, dielectric materials, piezoelectrics and in many other applications. The systematic synthetic chemistry and detailed structural understanding of refractory materials however is often extremely limited because of the intractable nature of the solids. Synthetic techniques are often limited to high temperature ceramic-type methods and the final products are typically insoluble powders. In many cases the understanding of properties of such materials would be aided greatly by a careful single crystal diffraction study, provided the materials can be prepared as high quality single crystals. The high temperature synthetic techniques are often problematic because they can contain lattice defects and/or site disorder among the various lattice positions of the metal ions.[1-3] Therefore, it is of great interest to develop alternative synthetic approaches to refractory oxides that enable low temperature reaction conditions as well as growth of high quality single crystals of the desired products. Our long-term goal is to develop the high temperature hydrothermal reaction method as a route to refractory oxides, particularly in the form of high quality single crystals.

We previously demonstrated that rare earth oxides can react with a variety of refractory tetravalent oxides in high temperature hydrothermal fluids to form a range of new materials including germanates and titanates.[4,5] The chemistry is extremely rich, and responsive to variations in synthetic conditions, particularly reactant stoichiometry and mineralizer. Of particular interest is the extension of this exploratory reaction chemistry to refractory pentavalent metal oxides such as Nb_2O_5 and Ta_2O_5. Our earlier work in the niobate system demonstrated that reactions in high temperature hydrothermal fluids led to formation of high quality single crystals of several

interesting materials including *RE*NbO_4.[6] It is of interest to develop analogous chemical reactions to rare earth tantalates as well. Tantalates have a considerable range of interesting physical properties. They can act as proton conductors,[7] ionic conducting oxides, catalysts for water splitting,[8,9] photoluminescent materials,[10,11] exhibit nonlinear optical behavior,[12,13] and perhaps most importantly serve as high dielectric materials.[14-17] Unfortunately, the synthetic approaches to metal tantalates are rather limited because of the intractable nature of tantalum oxides. Thus, the tantalates suffer from the synthetic challenges described above, and this has led to significant limitations in material development. The structural aspects of the tantalates seem to be particularly subtle and complex.[18] For example the parent oxide Ta_2O_5 is known to have an extremely complex lattice, and a detailed understanding of its structure is still a work in progress.[19] A synthetic procedure at modest temperatures leading to defect free single crystals would be extremely desirable. Additionally, the *RE*TaO_4 phases exhibit several structural complexities and can display a range of useful properties.[20-27] For example, the Lu analog $LuTaO_4$ is one of the densest oxides known and is thus a potentially useful host for scintillation detection.[28,29]

The hydrothermal method has been demonstrated to be useful for synthesizing several niobates and tantalates,[30-32] and represents an attractive approach because the relatively low reaction temperatures (≤700 ˚C) should minimize site disorder and defect formation. The present study seeks to explore the reaction chemistry of the early lanthanide oxides with tantalum oxide in various mineralizer fluids under suitable hydrothermal conditions. Given the nearly complete lack of background on reactions of these compounds we have to rely on exploratory investigations to determine the scope and limitations of the reaction conditions. In general, we found that high concentrations of hydroxide or fluoride mineralizers at temperatures between 600-700 ˚C afford sufficient solubility and reactivity to induce the formation of high quality single crystals of novel

products.[33,34] Previous work under these conditions using rare earth oxides and TiO_2 led to formation of well-known and important rare earth titanates such as $RE_2Ti_2O_7$, as well as a series of unusual rare earth titanate hydroxides with extremely complex structures.[5] Rare earth oxide building blocks often display fairly complex and subtle structural features,[35,36] and the present study extends our efforts to understand the fundamental descriptive reaction chemistry to the poorly explored combination of early rare earths and tantalum oxides.

2. EXPERIMENTAL SECTION

2.1. Hydrothermal Crystal Growth. In each reaction, approximately 0.2 g of reactants with 0.4 mL of 20-30 M KOH mineralizer was used. All the reactions were performed in 6 cm long silver ampoules with an outer diameter of 0.64 cm, filled to approximately a 60% of their free volume. The weld-sealed silver ampoules were loaded in to a Tuttle style autoclave and filled with distilled water at 80% of the free volume, to provide suitable counter pressure. The autoclave was heated to 650 °C for seven days at a typical pressure of 1.5 kbar. The crystals were retrieved after washing with de-ionized water. The chemicals used in this study were used as received, without further purification: La_2O_3 (Alfa Aesar, 99.999%), Pr_2O_3 (Alfa Aesar, 99.9%), Nd_2O_3 (Alfa Aesar,99.9%), Nb_2O_5 (Alfa Aesar, 99.9985%), Ta_2O_5 (Alfa Aesar, 99%). In all cases the use of lower mineralizer concentrations or lower temperatures led to reduced formation of the title compounds, as the lanthanide oxyhydroxide phases, *Ln*O(OH) were preferentially formed. The use of higher Ta_2O_5 contents in the reactions did not improve the yield of the title compounds, and any unreacted Ta_2O_5 was also present in those composite reaction products.

2.2. Synthesis of the Ln_2XO_5(OH) (*Ln* = La, Pr; *X* = Nb and Ta) Series. $La_2TaO_5(OH)$ was synthesized using a stoichiometric reaction of La_2O_3 and Ta_2O_5 in a 2:1 molar ratio with 30

M KOH. A typical reaction consisted of 0.1192 g of La_2O_3 and 0.0808 g of Ta_2O_5 with 0.4 mL of 30 M KOH. After the reaction period, clear, colorless crystals of $La_2TaO_5(OH)$ (Figure 1b) were obtained as the major product, with LaO(OH) occurring as a minor product (~10%). Isostructural $La_2NbO_5(OH)$ (clear polyhedra, Figure 1a) and $Pr_2TaO_5(OH)$ (green polyhedra, Figure 1c) were also grown in a similar fashion. It is interesting to mention that the 2:1 reaction between Pr_2O_3 and Ta_2O_5 reaction resulted 80% of green block-like crystals of $Pr_2TaO_5(OH)$ and 20% of green columnar crystals of $Pr_3Ta_2O_9(OH)$, Figure 1d. The yield of $La_2NbO_5(OH)$ was very low compared to the tantalate analogs, only forming ~30% $La_2NbO_5(OH)$ crystals, with the majority product being LaO(OH) single crystals.

2.3. Synthesis of the $Ln_3Ta_2O_9(OH)$ series (*Ln* = Pr and Nd). After the compound $Pr_3Ta_2O_9(OH)$ was determined as a minor product of the $Pr_2TaO_5(OH)$ synthesis, a stoichiometric reaction was performed to target higher yields of the $Pr_3Ta_2O_9(OH)$ crystals. These were synthesized using Pr_2O_3 and Ta_2O_5 in a 5:4 molar ratio with 30 M KOH. Herein, 0.0965 g of Pr_2O_3 and 0.1035 g of Ta_2O_5 were mixed with 0.4 mL of 30 M KOH. This reaction increased the yield of $Pr_3Ta_2O_9(OH)$ to 90% with a small amount of $Pr_2TaO_5(OH)$ remaining as a trace impurity. A similar reaction method was used to synthesize $Nd_3Ta_2O_9(OH)$, but in this case $Nd_3Ta_2O_9(OH)$ was the only product, observed in quantitative yield. After the completion of the reactions and filtration and washing with distilled water, flat columnar crystals of $Pr_3Ta_2O_9(OH)$ (green) and $Nd_3Ta_2O_9(OH)$ (lavender) crystals were recovered (Figure 1d & e).

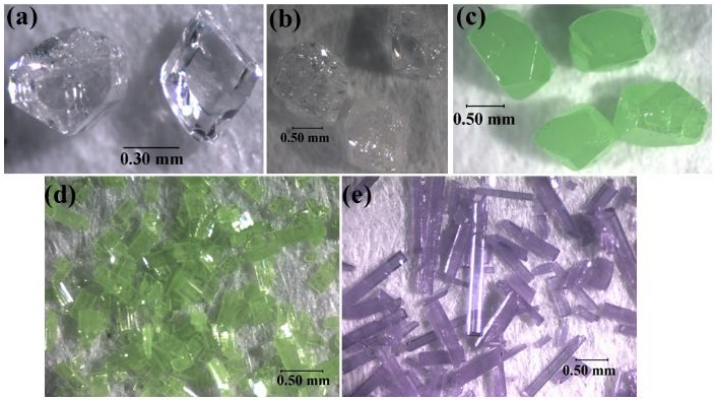

Figure 1. Hydrothermally grown crystals of (a) $La_2NbO_5(OH)$; (b) $La_2TaO_5(OH)$; (c) $Pr_2TaO_5(OH)$; (d) $Pr_3Ta_2O_9(OH)$; (e) $Nd_3Ta_2O_9(OH)$.

2.4. Characterization. Single crystal X-ray diffraction data were collected using a Rigaku AFC8 diffractometer equipped with a Mo Kα (λ = 0.71073 Å; graphite monochromated) sealed tube source and a Mercury CCD detector, and a Bruker D8 Venture diffractometer equipped with an Incoatec Mo Kα microfocus source and Photon 100 CMOS detector. All the single crystal data were collected at room temperature using phi and omega scans with a width of 0.5 degrees. Data were processed using the Apex3[37] and CrystalClear[38] software packages and corrected for absorption and Lorentz and polarization effects. Space group determinations were made based on the systematic absences. The structures were solved by direct methods and subsequently refined using full-matrix least squares techniques within the SHELXTL software suite.[39] All non-hydrogen atoms were refined anisotropically. The presence of hydroxide groups necessary for charge balance were confirmed with the IR spectrum and bond valence calculations, and appropriate hydrogen atoms were then identified from the difference electron density map and their distances restrained to an appropriate distance from the parent oxygen atom. The crystallographic data of the $La_2NbO_5(OH)$, $La_2TaO_5(OH)$ and $Pr_2TaO_5(OH)$ series and the $Pr_3Ta_2O_9(OH)$ and $Nd_3Ta_2O_9(OH)$ series are presented in Table 1 and Table 2, respectively. Similarly, selected interatomic distances for the two series of compounds are given in Table 3 and

Table 4, respectively. Structures were deposited with the joint CCDC/FIZ Karlsruhe deposition service, deposition numbers CCDC 1888860-1888864.

The infrared spectra were collected using a Nicolet Magna IR Spectrometer 550 in the frequency range from 400 cm^{-1} to 4000 cm^{-1} with a 4 cm^{-1} resolution (ESI, Figure SI 1) using the KBr pellet technique. Absorption spectra were obtained from a PC-controlled SHIMADZU UV-3600 UV/vis/near-IR spectrometer equipped with an integrating sphere (ISR-3100). Well-ground single crystals were smeared onto $BaSO_4$ plates for data collection. The reflectance data was collected in the range of 200-2000 nm and converted to absorption by using the Kubelka-Munk Function. Transitions in the visible and near infrared regions were characteristic of the lanthanide elements present in each compound (ESI, Figure SI 2). Absorption measurements into the UV region indicated band gaps around 4 eV for $Pr_3Ta_2O_9(OH)$ and $Nd_3Ta_2O_9(OH)$ (ESI, Figure SI 3).

Energy dispersive spectroscopy analysis (EDS) was performed using a Hitachi S-3400 scanning electron microscope equipped with an OXFORD EDX microprobe (ESI, Table S1). Further, powder X-ray diffraction (PXRD) was performed using a Rigaku Ultima IV diffractometer with CuK_α radiation (λ= 1.5406 Å) at 0.02° intervals at a rate of 0.1°/min from 5-65° and the PXRD pattern of selected ground single crystals are given in Figure 2. These patterns were in good agreement with the expected patterns calculated on the basis of the single crystal structure refinement.

Table 1. Crystallographic data of $Ln_2XO_5(OH)$ (X = Nb, Ta) from single crystal X-ray diffraction.

	1	**2**	**3**
empirical formula	$La_2NbO_5(OH)$	$La_2TaO_5(OH)$	$Pr_2TaO_5(OH)$
formula weight (g/mol)	467.74	555.78	559.78
crystal system	monoclinic	monoclinic	monoclinic
space group, Z	$P2_1/n$ (no.14), 4	$P2_1/n$ (no.14), 4	$P2_1/n$ (no.14), 4
temperature, °C	25	25	25
crystal size (mm)	0.12 x 0.06 x 0.06	0.08 x 0.06 x 0.06	0.08 x 0.06 x 0.06
a, Å	7.0987(17)	7.0897(3)	7.0137(3)
b, Å	6.8056(18)	6.7199(4)	6.7134(3)
c, Å	10.259(3)	10.2645(5)	10.1240(4)
β, °	94.345(9)	94.158(2)	94.122(2)
volume, Å^3	494.2(2)	487.73(4)	475.46(3)
calcd density (g/cm^3)	6.286	7.569	7.820
absorption coefficient (mm^{-1})	19.203	39.526	43.070
F(000)	816	944	960
Tmax, Tmin	1.0000, 0.8691	1.0000, 0.2900	1.0000, 0.3510
Θ range for data	3.37-25.24	3.38-26.50	3.42-25.50
reflections collected	4022	9192	5479
data/restraints/parameters	899/1/86	1013/1/86	887/1/86
final R [I> 2σ(I)] R1, wR2	0.0247, 0.0580	0.0166, 0.0365	0.0160, 0.0384
final R (all data) R1, wR2	0.0255, 0.0585	0.0181, 0.0370	0.0169/0.0389
goodness-of-fit on F^2	1.149	1.180	1.118
largest diff. peak/hole, e/ Å^3	1.249/-2.508	0.814/-0.887	1.194/-0.999

Table 2. Crystallographic data of $Pr_3Ta_2O_9(OH)$ and $Nd_3Ta_2O_9(OH)$ determined by single crystal X-ray diffraction.

	4	**5**
empirical formula	$Pr_3Ta_2O_9(OH)$	$Nd_3Ta_2O_9(OH)$
formula weight (g/mol)	945.64	955.63
crystal system	orthorhombic	orthorhombic
space group, *Z*	*Pnnm* (no.58), 4	*Pnnm* (no.58), 4
temperature, °C	25	25
crystal size (mm)	0.10 x 0.06 x 0.06	0.10 x 0.06 x 0.06
a, Å	19.3603(10)	19.3122(8)
b, Å	5.5779(3)	5.5525(2)
c, Å	7.7079(3)	7.6800(3)
volume, $Å^3$	832.37(7)	823.53(6)
calcd density (g/cm^3)	7.546	7.708
absorption coefficient (mm^{-1})	43.454	45.086
F(000)	1616	1628
Tmax, Tmin	1.0000, 0.4857	1.0000, 0.2760
Θ range for data	2.10-25.49	2.85-25.49
reflections collected	14191	11500
data/restraints/parameters	840/1/79	827/1/79
final R [$I > 2\sigma(I)$] R1, wR2	0.0208, 0.0434	0.0214, 0.0501
final R (all data) R1, wR2	0.0263, 0.0452	0.0237, 0.0509
goodness-of-fit on F^2	1.047	1.176
largest diff. peak/hole, e/ $Å^3$	1.098/-1.388	1.398/-1.380

Table 3. Selected bond lengths (Å) in the $Ln_2XO_5(OH)$ (X = Nb and Ta) series of compounds.

$La_2NbO_5(OH)$					
La(1)O_8		**La(2)O_9**		**Nb(1)O_6**	
La(1)−O(1)	2.569(5)	La(2)−O(1)	2.490(5)	Nb(1)−O(1)	2.066(5)
La(1)−O(2)	2.583(5)	La(2)−O(2)	2.603(5)	Nb(1)−O(1)	2.169(5)
La(1)−O(3)	2.419(5)	La(2)−O(2)	2.735(5)	Nb(1)−O(2)	1.936(5)
La(1)−O(3)	2.498(5)	La(2)−O(3)	2.586(5)	Nb(1)−O(3)	1.970(5)
La(1)−O(4)	2.623(5)	La(2)−O(4)	2.464(5)	Nb(1)−O(5)	2.011(5)
La(1)−O(4)	2.633(5)	La(2)−O(4)	2.810(5)	Nb(1)−O(6)	1.871(5)
La(1)−O(5)	2.506(5)	La(2)−O(5)	2.501(5)		
La(1)−O(6)	2.547(5)	La(2)−O(5)	2.650(5)		
		La(2)−O(6)	2.616(5)		
$La_2TaO_5(OH)$					
La(1)O_8		**La(2)O_9**		**Ta(1)O_6**	
La(1)−O(1)	2.526(5)	La(2)−O(1)	2.505(4)	Ta(1)−O(1)	2.072(4)
La(1)−O(2)	2.510(4)	La(2)−O(2)	2.571(4)	Ta(1)−O(1)	2.120(4)
La(1)−O(3)	2.434(5)	La(2)−O(2)	2.720(4)	Ta(1)−O(2)	1.928(4)
La(1)−O(3)	2.524(4)	La(2)−O(3)	2.521(4)	Ta(1)−O(3)	1.972(4)
La(1)−O(4)	2.538(4)	La(2)−O(4)	2.462(4)	Ta(1)−O(5)	2.000(4)
La(1)−O(4)	2.651(4)	La(2)−O(4)	2.753(4)	Ta(1)−O(6)	1.883(5)
La(1)−O(5)	2.502(4)	La(2)−O(5)	2.521(5)		
La(1)−O(6)	2.555(5)	La(2)−O(5)	2.713(6)		
		La(2)−O(6)	2.544(5)		
$Pr_2TaO_5(OH)$					
Pr(1)O_8		**Pr(2)O_9**		**Ta(1)O_6**	
Pr(1)−O(1)	2.552(4)	Pr(2)−O(1)	2.462(5)	Ta(1)−O(1)	2.050(4)
Pr(1)−O(2)	2.524(4)	Pr(2)−O(2)	2.544(5)	Ta(1)−O(1)	2.138(4)
Pr(1)−O(3)	2.365(4)	Pr(2)−O(2)	2.731(4)	Ta(1)−O(2)	1.941(4)
Pr(1)−O(3)	2.458(5)	Pr(2)−O(3)	2.539(5)	Ta(1)−O(3)	1.975(5)
Pr(1)−O(4)	2.577(5)	Pr(2)−O(4)	2.427(5)	Ta(1)−O(5)	2.003(5)
Pr(1)−O(4)	2.598(5)	Pr(2)−O(4)	2.766(5)	Ta(1)−O(6)	1.886(5)
Pr(1)−O(5)	2.453(4)	Pr(2)−O(5)	2.460(5)		
Pr(1)−O(6)	2.500(5)	Pr(2)−O(5)	2.629(5)		
		Pr(2)−O(6)	2.541(5)		

Table 4. Selected bond lengths (Å) in $Pr_3Ta_2O_9(OH)$ and $Nd_3Ta_2O_9(OH)$.

$Pr_3Ta_2O_9(OH)$		$Nd_3Ta_2O_9(OH)$	
Pr(1)O_8		**Nd(1)O_8**	
Pr(1)−O(1) x 2	2.516(6)	Nd(1)−O(1) x 2	2.494(6)
Pr(1)−O(4) x 2	2.544(5)	Nd(1)−O(4) x 2	2.536(5)
Pr(1)−O(5) x 2	2.465(6)	Nd(1)−O(5) x 2	2.449(5)
Pr(1)−O(6)	2.434(8)	Nd(1)−O(6)	2.410(8)
Pr(1)−O(7)	2.497(9)	Nd(1)−O(7)	2.469(8)
Pr(2)O_7		**Nd(2)O_7**	
Pr(2)−O(2) x 2	2.322(9)	Nd(2)−O(2) x 2	2.299(8)
Pr(2)−O(3)	2.457(8)	Nd(2)−O(3)	2.424(8)
Pr(2)−O(4) x 2	2.437(6)	Nd(2)−O(4) x 2	2.426(5)
Pr(2)−O(5) x 2	2.541(6)	Nd(2)−O(5) x 2	2.536(6)
Pr(3)O_8		**Nd(3)O_8**	
Pr(3)−O(2) x 2	2.347(5)	Nd(3)−O(2) x 2	2.340(5)
Pr(3)−O(4) x 2	2.610(6)	Nd(3)−O(4) x 2	2.590(6)
Pr(3)−O(5) x 2	2.521(6)	Nd(3)−O(5) x 2	2.513(5)
Pr(3)−O(6) x 2	2.497(5)	Nd(3)−O(6) x 2	2.491(5)
Ta(1)O_6		**Ta(1)O_6**	
Ta(1)−O(1)	1.966(5)	Ta(1)−O(1)	1.967(5)
Ta(1)−O(1)	2.062(5)	Ta(1)−O(1)	2.065(5)
Ta(1)−O(3)	1.986(2)	Ta(1)−O(3)	1.985(2)
Ta(1)−O(4)	1.917(6)	Ta(1)−O(4)	1.916(5)
Ta(1)−O(5)	1.995(5)	Ta(1)−O(5)	1.992(5)
Ta(1)−O(7)	1.999(2)	Ta(1)−O(7)	1.998(2)

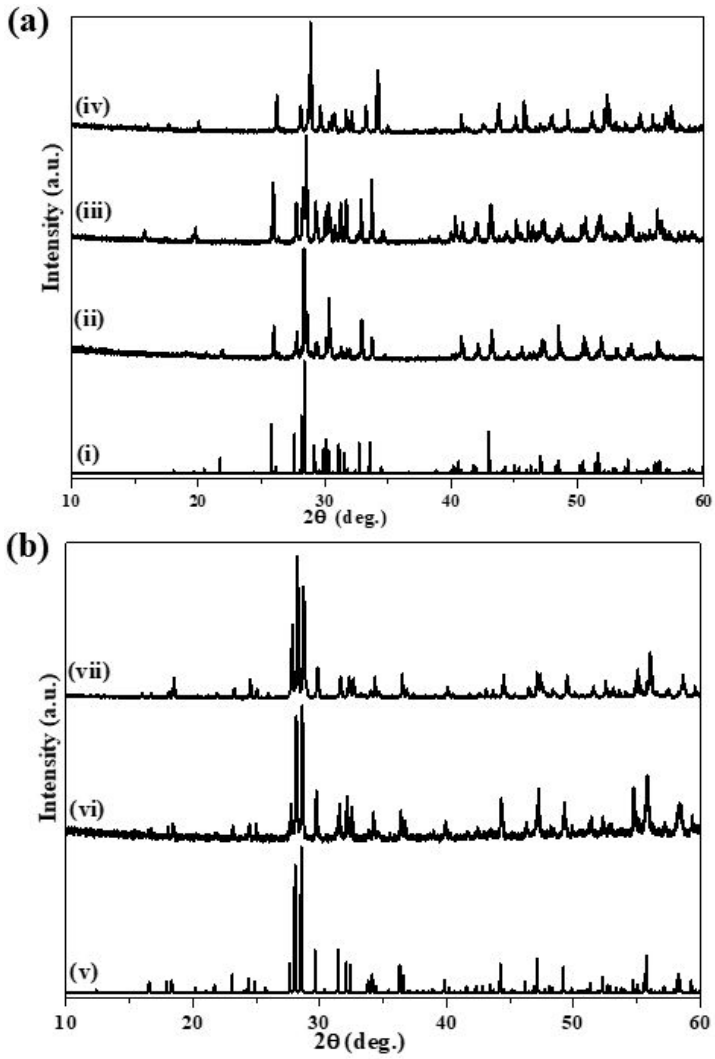

Figure 2. Powder diffraction patterns of the $La_2NbO_5(OH)$, $La_2TaO_5(OH)$, $Pr_2TaO_5(OH)$ series (A) and $Pr_3Ta_2O_9(OH)$ and $Nd_3Ta_2O_9(OH)$ series (B): (i) calculated PXRD pattern of $La_2NbO_5(OH)$ based on the single crystal structure, (ii) observed pattern for $La_2NbO_5(OH)$, (iii) observed pattern for $La_2TaO_5(OH)$, (iv) observed pattern for $Pr_2TaO_5(OH)$, (v) calculated PXRD pattern of $Pr_3Ta_2O_9(OH)$ based on the single crystal structure, (vi) observed pattern for $Pr_3Ta_2O_9(OH)$, (vii) observed pattern for $Nd_3Ta_2O_9(OH)$.

3. RESULTS AND DISCUSSION

3.1 Crystal Structure of the $Ln_2XO_5(OH)$ (*Ln* = La, Pr, Nd. *X* = Nb and Ta) Series.

The $Ln_2XO_5(OH)$ compounds form an isomorphous series for the Nb and Ta analogs, crystallizing in the monoclinic crystal system with the space group $P2_1/n$. The unit cell parameters and selected bond lengths are given in Tables 1 and 3, respectively. The structure of $La_2TaO_5(OH)$ will be discussed in detail as a representative example of the structure type. The structure is a complex, dense three dimensional framework (Figure 3). There are two crystallographically distinct La atoms and one unique Ta atom located on general positions. The framework of $La_2TaO_5(OH)$ is constructed of corner- and edge-sharing of LaO_n (n = 8 and 9) polyhedra and TaO_6 octahedra. The structure can be divided into two structural units based on lanthanum oxide and tantalum oxide interactions. Figure 4 further divides the 3-D La−O−La framework into two subunits, consisting of a fusion of La(1)−O−La(1) chains with La(2)−O−La(2) layers (Figure 4a, 4b). Edge-sharing chains of $La(1)O_8$ polyhedra propagate via shared O(3) and O(4) atoms resulting in infinite zigzag chains along the *b*-axis (Figure 4c). The $La(2)O_9$ units share edges via O(4) and corners via O(2), forming two-dimensional La(2)−O−Ln(2) layers (Figure 4d). The subunits are fused via La(1)−O−La(2) edge sharing of O(4) and O(6) and face sharing of O(2), O(3), and O(5) to form the complex 3-D La−O−La framework where La(1) chains are sandwiched between La(2) sheets (Figure 4b). The light color for all the products that represent the characteristic colors of the rare earth ions (colorless for La, pale violet for Nd and apple green for Pr) strongly suggests that the tantalates ions are all pentavalent. The presence of one hydroxide group is necessitated by charge balance considerations, and was confirmed using infrared spectroscopy (SI, Figure S1). The O(4) atom only has bonds to La atoms, with none to Ta atoms, so is underbonded with respect to its bond valence sum, and thus is assigned as the location of the OH^- group in the structure.

The second part of the structure is built from tantalate octahedra that form edge-shared Ta_2O_{10} dimers via O(1) and its symmetry-related partner (Figure 5). These dimers occupy gaps in the 3-D La−O−La oxide lattice to form the dense La−O−Ta framework. The bridging Ta-O bonds within the Ta_2O_{10} dimers are noticeably elongated compared to those forming the Ta−O−La frameworks, causing the octahedra to be rather distorted (Table 3). The corresponding isostructural niobate $La_2NbO_5(OH)$ was prepared for comparison purposes and the average Nb−O bond length is 2.004(5) Å compared to the average Ta−O bond lengths for $La_2TaO_5(OH)$ and $Pr_2Ta_5O(OH)$ of 1.996(6) Å and 1.999(6) Å, respectively. However, the bridging Nb−O bonds in $La_2NbO_5(OH)$ exhibit somewhat greater anisotropy (Nb-O = 2.169(5) Å and 2.066(5) Å) than the same Ta−O bonds in $La_2TaO_5(OH)$ (Ta-O = 2.120(4) Å and 2.072(4) Å) and $Pr_2TaO_5(OH)$ (Ta-O = 2.138(4) Å and 2.050(4) Å). The average *Ln*−O bond distances in $La_2NbO_5(OH)$, $La_2TaO_5(OH)$ and $Pr_2Ta_5O(OH)$ are 2.577(6), 2.560(6) and 2.535(6) Å, respectively.

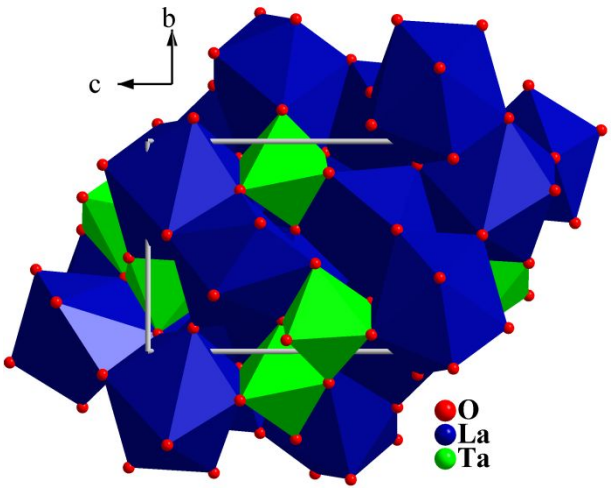

Figure 3. A view of $La_2TaO_5(OH)$ along the *a*-axis illustrating the complex nature of the packed structure. LaO_n and TaO_6 polyhedra represent in blue and green polyhedra, respectively.

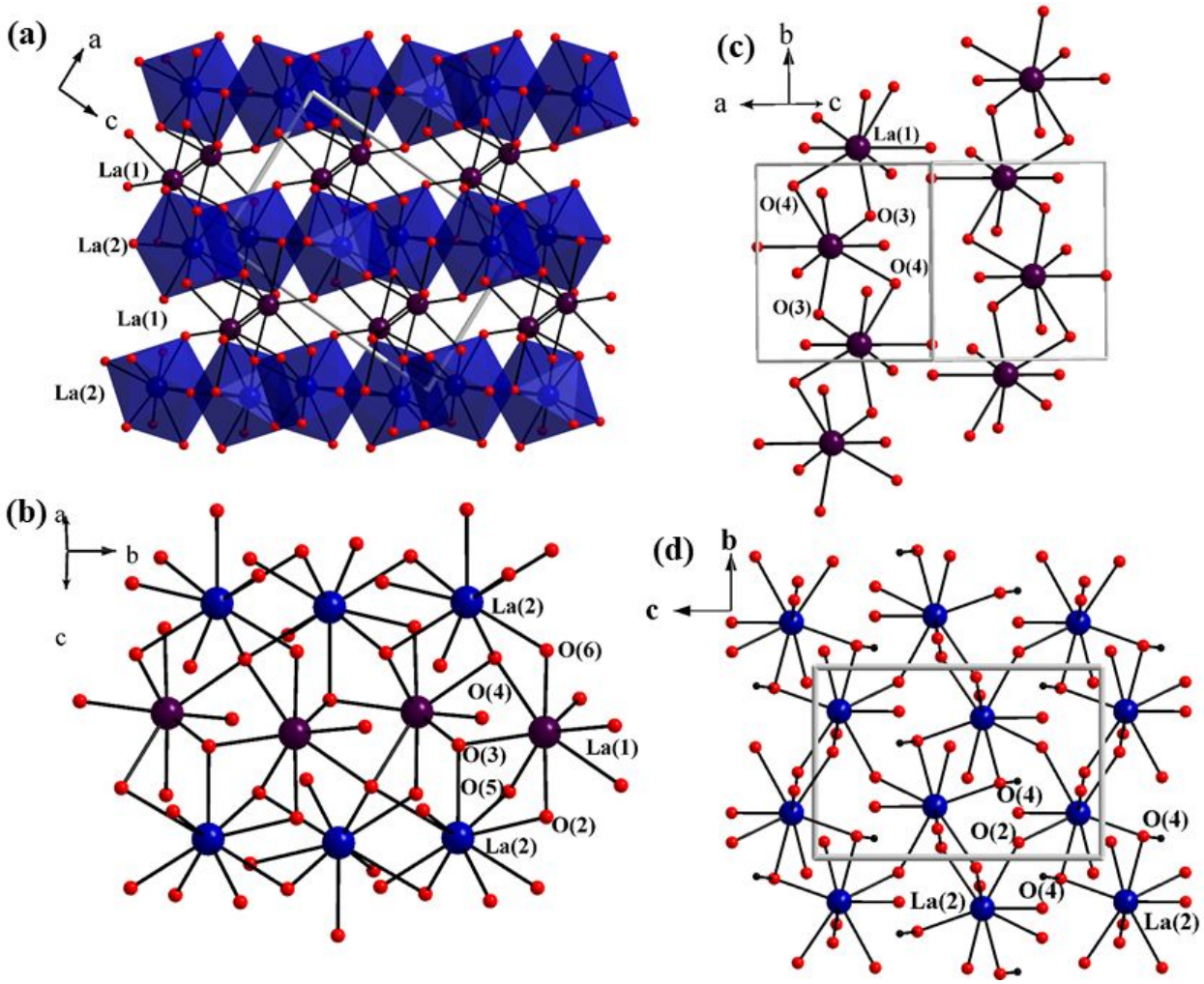

Figure 4. The La−O−La 3-D framework of $La_2TaO_5(OH)$. (a) The La−O−La 3-D framework is constructed from chains of La(1)−O−La(1) and layers of La(2)−O−La(2) which are interconnected in alternating fashion; (b) connectivity between $La(1)O_8$ and $La(2)O_9$ via O(2), O(3), O(4) and O(5) atoms; (c) Partial structure of La(1)−O−La(1) chains propagating along the *b*-axis; (d) Partial structure of La(2)−O−La(2) layers along the *bc*-plane. These chains and layers are interconnected with each other giving the overall 3-D La−O−La lattice. The hydrogen atom positions are omitted for clarity in (a-c), but included in (d) to show the nature of the OH group on the O(4) atom.

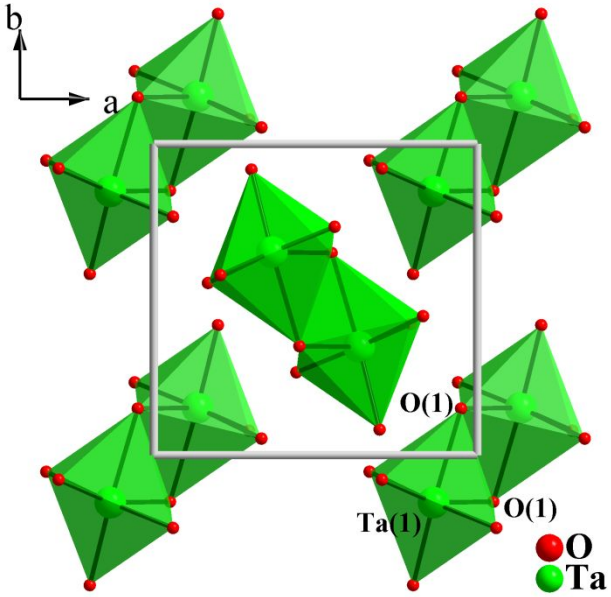

Figure 5. Edge-shared dimers of TaO_6-octahedra in $La_2TaO_5(OH)$. These dimers are embedded in the 3-D La−O−La lattice to give a very dense overall structure.

3.2. Crystal Structure of $Ln_3Ta_2O_9(OH)$ (*Ln* = Pr, Nd). The compounds $Pr_3Ta_2O_9(OH)$ and $Nd_3Ta_2O_9(OH)$ are isostructural and crystallize in the orthorhombic space group *Pnnm* (no.58), with lattice parameters a = 19.3603(10) Å, b = 5.5769(3) Å, c = 7.7079(3) Å for $Pr_3Ta_2O_9(OH)$ and a = 19.3122(8) Å, b = 5.5525(3) Å, c = 7.6800(6) Å for $Nd_3Ta_2O_9(OH)$. Crystallographic data is given in Table 2 and selected bond lengths are listed in Table 4. This series of compounds also possesses a complicated 3-D framework, and the $Pr_3Ta_2O_9(OH)$ structure will be discussed in detail as the representative example. The 3-D structure of $Pr_3Ta_2O_9(OH)$ is shown in Figure 6 and can be broken down into two 2-D sublattices of Pr−O−Pr and Ta−O−Ta slabs. The 2-D slabs of Pr−O−Pr and Ta−O−Ta extend in the *bc* plane, and occur in alternating fashion along the *a*-axis. The Pr−O−Pr slabs (Figure 6b) are composed of three crystallographically distinct PrO_n polyhedra, $Pr(1)O_8$, $Pr(2)O_7$, and $Pr(3)O_8$. There is only one crystallographically unique Ta atom, forming a TaO_6 unit, from which the Ta-O-Ta slabs (Figure 6c) are constructed.

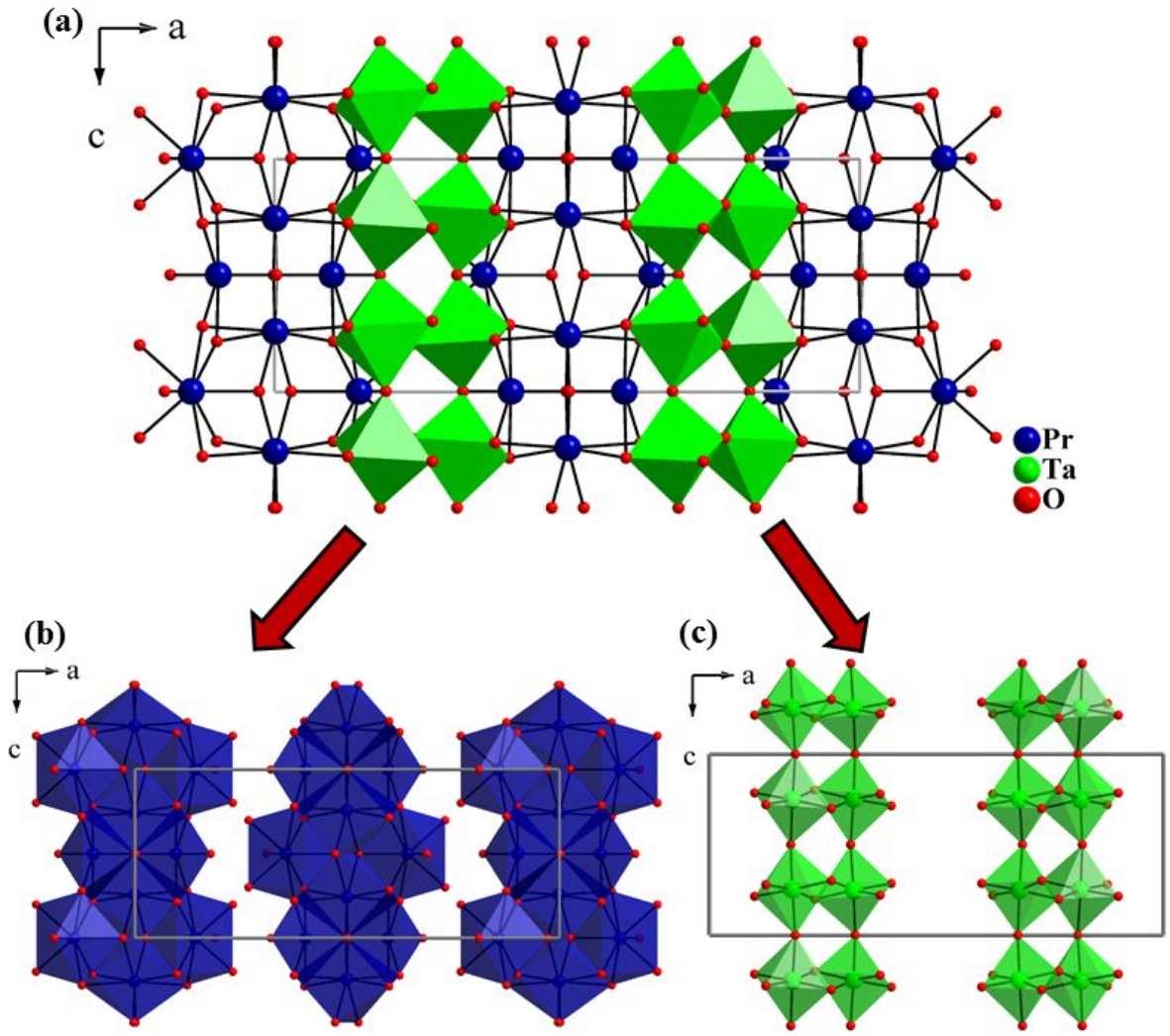

Figure 6. Illustration of Pr−O−Pr and Ta−O−Ta building units in $Pr_3Ta_2O_9(OH)$. (a) Construction of the $Pr_3Ta_2O_9(OH)$ structure from two basic units of 2-D Pr−O−Pr and Ta−O−Ta slabs; (b) arrangement of the 2-D Pr−O−Pr layers (extending in the *bc* plane) within the unit; (c) packing of isolated Ta−O−Ta slabs (also extending in the *bc* plane) within the unit cell.

The Pr−O−Pr slabs themselves are a complex 2-D lattice, detailed in Figure 7a. Figure 7b-d further divides these slabs into simpler constructs. The $Pr(3)O_8$ polyhedra build the backbone of the 2-D lattice by forming edge-sharing chains with one another along the *c*-axis, via O(2) and O(6) bridging atoms (Figure 7c). The $Pr(1)O_8$ and $Pr(2)O_7$ polyhedra form their own edge-sharing chains that flank the $Pr(3)O_8$ chains, also running parallel to the *c*-axis. In this way Pr(1) is oxygen

edge- and corner- sharing with Pr(3) atoms (Figure 7b) and Pr(2) is oxygen edge-sharing with Pr(3) (Figure 7d). The staggered arrangement of these two types of chains along both the *a*- and *b*-axes leads to the 2-D Pr−O−Pr sublattice three Pr atoms thick along the *a*-axis. Along the *a*-axis, two $Pr(2)O_7$ polyhedra are also edge-sharing with one another via two bridging O(2) oxygen atoms that act as μ_4-oxo vertices. The other oxygen atom that is fully-contained within the Pr−O−Pr slab is O(6), which, acting as a μ_3-oxo vertex between one $Pr(1)O_8$ and two $Pr(3)O_8$ polyhedra, has an underbonded bond valence sum, and is assigned as the site of the OH^- group in the structure. As in $Ln_2TaO_5(OH)$ above, the presence of a proton is required by charge balance considerations and was also confirmed by infrared spectroscopy (SI, Figure S1). The average bond lengths of $Pr_3Ta_2O_9(OH)$: Pr(1)−O, Pr(2)−O and Pr(3)−O are 2.448(8) Å, 2.434(8) Å, 2.498(8) Å, $Nd_3Ta_2O_9(OH)$: Nd(1)−O, Nd(2)−O and Nd(3)−O are 2.479(8) Å, 2.442(8) Å, 2.480(8) Å.

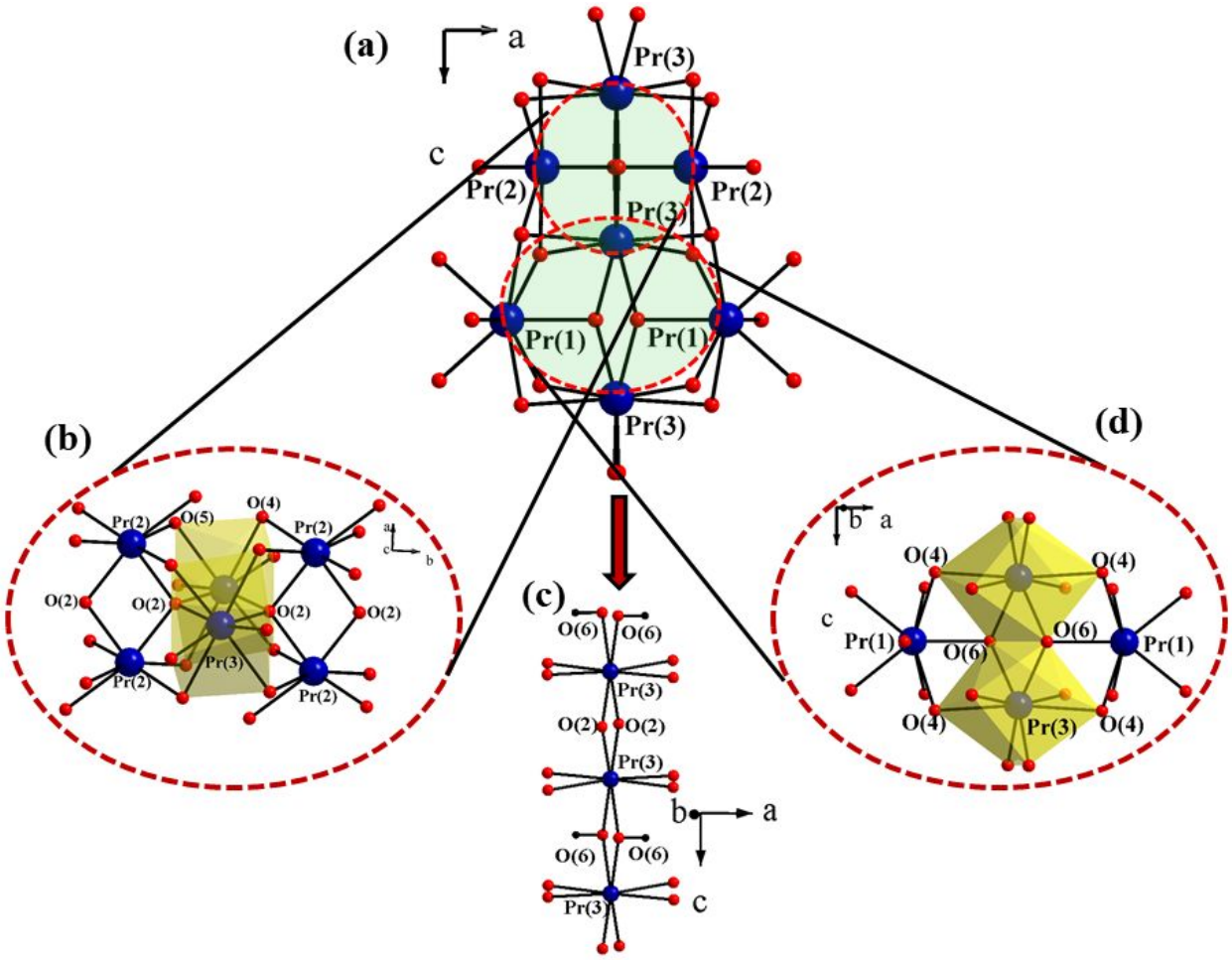

Figure 7. (a) Building blocks of the 2-D Pr−O−Pr slab in $Pr_3Ta_2O_9(OH)$ structure; (b) shows the connectivity between $Pr(2)O_7$ and $Pr(3)O_8$ polyhedra; (c) edge-sharing chains made from $Pr(3)O_8$ polyhedra; (d) connectivity between $Pr(3)O_8$ polyhedra and $Pr(1)O_8$ polyhedra. The hydrogen atom attached to O(6) is omitted from figures (a), (b), and (d) for clarity, but shown in part (c) to show its orientation on the chains.

The Ta−O−Ta slabs in $Pr_3Ta_2O_9(OH)$ are a somewhat simpler construction, also extending in the *bc*-plane. The slab is corrugated, having a thickness of two Ta atoms along the *a*-axis. The slabs are built from corner-sharing TaO_6 octahedra (Figure 8), occurring via O(3) and O(7) along the *c*-axis, and O(1) along the *b*-axis. The Ta−O bond lengths of $Pr_3Ta_2O_9(OH)$ and $Nd_3Ta_2O_9(OH)$ range from 1.895 to 2.063 Å and from 1.911 to 2.068 Å, respectively, indicating moderate distortion of the TaO_6 octahedra. The Ta−O−Ta slabs are fused to Pr−O−Pr slabs by edge- and corner-sharing of oxygen atoms.

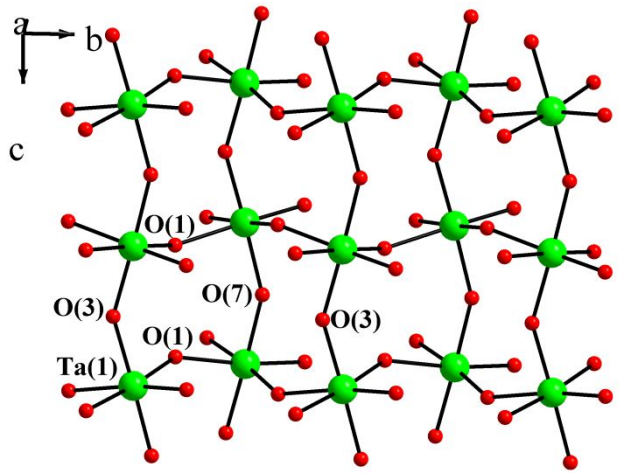

Figure 8. The 2-D lattice of Ta−O−Ta in $Pr_3Ta_2O_9(OH)$.

Interestingly, this structure type bears some important similarity to that of $La_5Ti_4O_{15}(OH)$, which we recently discovered as part of a similar synthetic and structural survey of the lanthanide titanates.[5] Both $Pr_3Ta_2O_9(OH)$ (Figure 9a, 9c, 9d) and $La_5Ti_4O_{15}(OH)$ (Figure 9b, 9e, 9f) crystallize in space group *Pnnm*, and have nearly identical *b* and *c* lattice parameters, while the *a*-axis is elongated by over 50% for $La_5Ti_4O_{15}(OH)$ (*a* = 30.5152(12) Å, *b* = 5.5832(2) Å, *c* = 7.7590(10) Å). The structure of $La_5Ti_4O_{15}(OH)$ is also a complex framework of a 3-D La−O−La sublattice with 2-D Ti−O−Ti slabs. The La−O−La sublattice is constructed from five unique La sites. However, three of these sites form a nearly identical subunit slab to that in $Pr_3Ta_2O_9(OH)$ (Figures 9c, 9e). The remaining two unique La sites in $La_5Ti_4O_{15}(OH)$ can be thought of as spacers between these slabs. The Ti−O−Ti slab sublattice is likewise expanded in $La_5Ti_4O_{15}(OH)$ to be four Ti atoms thick along the *a*-axis, compared to two Ta atoms thick in the Ta−O−Ta slab sublattice of $Pr_3Ta_2O_9(OH)$ (Figures 9d, 9f). These extra Ti atoms in the $La_5Ti_4O_{15}(OH)$ slabs are effectively inserted between the locations of the two Ta atoms of the $Pr_3Ta_2O_9(OH)$ slabs such that the extra atoms of the thicker slab overlap (and interconnect with) the extra La−O−La spacer region also present in $La_5Ti_4O_{15}(OH)$. From a crystal chemistry standpoint, the extra inserted unit of $[La_2Ti_2O_6]^{2+}$ is offset by the replacement of the two Ta^{5+} octahedra in $Pr_3Ta_2O_9(OH)$ with Ti^{4+}

octahedra in $La_5Ti_4O_{15}(OH)$. In this way, a related structural series of the tetravalent and pentavalent transition metals (TM) with lanthanides (Ln) can be envisioned as $Ln_nTM_{n-1}O_{3n}(OH)$ for n = 3-5.

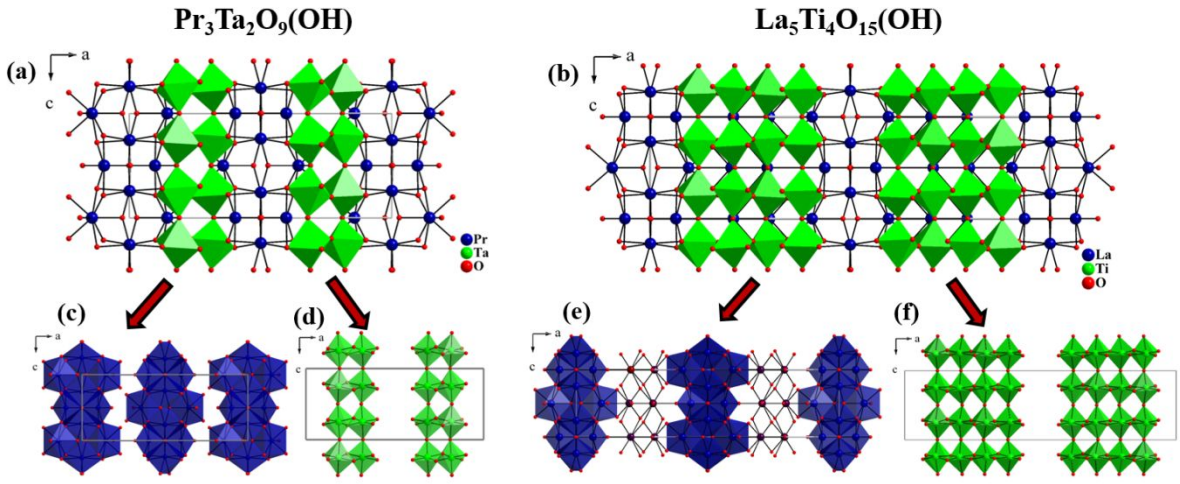

Figure 9. Structural comparison of (a) $Pr_3Ta_2O_9(OH)$ and (b) $La_5Ti_4O_{15}(OH)$ showing the elongation along *a*-axis; (c) isolated Pr−O−Pr slabs propagate in the *bc* plane; (d) isolated Ta−O−Ta slabs propagate along the *bc* plane; (e) 3-D La−O−La framework; blue polyhedra highlight the 2-D slabs similar to those in (c), and separated by additional La−O−La spacers; (f) Ti−O−Ti slabs propagate along the *bc* plane.

4. CONCLUSION

The work reports an initial examination of the reactions of the early rare earth oxides with Ta_2O_5 in high temperature hydrothermal fluids. We wish to examine reactions of all rare earth oxides in systematic fashion with the long-term goals of both unearthing new chemistry, and also developing a useful route to rare earth tantalate single crystals. These initial results indicate that concentrated hydroxides (20-30 M OH^-) are useful growth media for inducing reactivity of such refractory oxides. This is where a broad understanding of the descriptive chemistry is generally lacking in the literature, so an examination of the most fundamental reactions of just the simple oxides yields interesting new products. Novel compounds with the formulas $Ln_2Ta_2O_5(OH)$ and

$Ln_3Ta_2O_9(OH)$ (*Ln* = La-Nd) grow easily as large high quality single crystals and have complex crystal structures containing a variety of two-dimensional slabs built of edge shared rare earth oxide and tantalum oxide octahedral building blocks. The various slabs of lanthanide oxides and tantalum oxides form interpenetrating structures of different types leading to dense complicated three-dimensional lattices. The role of the hydroxide in the structure formation is not fully understood at this time, though it is necessary for charge balance. In general the location of the hydroxide in the lattice seems to be well ordered in all cases but does not appear to be a critical driver in the structure formation. We believe that the primary factor in the growth of these complex structures is the interpenetrating slabs formed by the various edge sharing polyhedra. As complex and unusual as these structures appear to be, they share a curious structural relationship with a series of rare earth titanates formed under similar synthetic conditions. Having suitably demonstrated that the hydrothermal fluids are excellent fluids for the growth of novel rare earth tantalate hydroxides, our next steps will attempt to determine the scope and limitations of the hydrothermal reaction media with the rare earth tantalates. This includes a systematic examination of the descriptive chemistry of the remaining lanthanide oxides with tantalum oxide, and attempts to grow single crystals of anhydrous lanthanide tantanlates such as $LnTaO_4$.

■ ACKNOWLEDGEMENTS

We are indebted to the Department of Energy Basic Energy Sciences, Award Number DE-SC0014271, for support of this work.

■ CONFLICT OF INTEREST

There are no conflicts to declare.

■ REFERENCES

(1) Navrotsky, A. Thermochemical insights into refractory ceramic materials based on oxides with large tetravalent cations. *J. Mater. Chem.* **2005**, *15*, 1883–1890.

(2) Mugavero, S. J.; Gemmill, W. R.; Roof, I. P.; zur Loye, H.-C. Materials Discovery by Crystal Growth: Lanthanide Metal Containing Oxides of the Platinum Group Metals (Ru,Os,Ir,Rh,Pd,Pt) from Molten Alkali Metal Hydroxides. *J. Solid State Chem.* **2009**, *182*, 1950–1963.

(3) Bugaris, D. E.; zur Loye, H.-C. Materials Discovery by Flux Crystal Growth: Quaternary and Higher Order Oxides. *Angew. Chem. Int. Ed.* **2012**, *51*, 3780–3811.

(4) Fulle, K.; Sanjeewa, L. D.; McMillen, C. D.; Wen, Y.; Rajamanthrilage, A. C.; Anker, J. N.; Chumanov, G.; Kolis, J. W. One-Pot Hydrothermal Synthesis of $Tb^{III}_{13}(GeO_4)_6O_7(OH)$ and $K_2Tb^{IV}Ge_2O_7$: Preparation of a Stable Terbium(4+) Complex. *Inorg. Chem.* **2017**, *56*, 6044−6047.

(5) Fulle, K.; Sanjeewa, L.D.; McMillen, C.D.; Kolis, J.W. High Temperature Hydrothermal Synthesis of Rare-Earth Titanates: Synthesis and Structure of $RE_5Ti_4O_{15}(OH)$ (*RE* = La, Er), $Sm_3TiO_5(OH)_3$, $RE_5Ti_2O_{11}(OH)$ (*RE* = Tm-Lu) and $Ce_2Ti_4O_{11}$. *Dalton Trans.* **2018**, *47*, 6754-6762.

(6) Fulle, K.; McMillen, C. D.; Sanjeewa, L. D.; Kolis, J. W. Hydrothermal Chemistry and Growth of Fergusonite-type $RENbO_4$ (*RE* = La−Lu, Y) Single Crystals and New Niobate Hydroxides. *Cryst. Growth Des.* **2016**, *16*, 4910−4917.

(7) Kreuer, K. D. Proton-Conducting Oxides. *Annu. Rev. Mater. Res.* **2003**, *33* (1), 333–359.

(8) Osterloh, F. E. Inorganic Materials as Catalysts for Photochemical Splitting of Water. *Chem. Mater.* **2008**, *20* (1), 35–54.

(9) Abe, R.; Higashi, M.; Zou, Z.; Sayama, K.; Abe, Y.; Arakawa, H. Photocatalytic Water Splitting into H_2 and O_2 over R_3TaO_7 and R_3NbO_7 (R = Y, Yb, Gd, La): Effect of Crystal Structure on Photocatalytic Activity. *J. Phys. Chem. B* **2004**, *108*, 811–814.

(10) Roof, I. P.; Jagau, T.-C.; Zeier, W. G.; Smith, M. D.; zur Loye, H.-C. Crystal Growth of a New Series of Complex Niobates, $LnKNaNbO_5$ (Ln = La, Pr, Nd, Sm, Eu, Gd, and Tb): Structural Properties and Photoluminescence. *Chem. Mater.* **2009**, *21*, 1955-1961.

(11) Roof, I. P.; Smith, M. D.; Park, S.; zur Loye, H.-C. $EuKNaTaO_5$: Crystal Growth, Structure and Photoluminescence Property. J. Am. Chem. Soc. **2009**, *131*, 4202-4203.

(12) Korotkov, A. S.; Atuchin, V. V. Distribution, Structures and Nonlinear Properties of Noncentrosymmetric Niobates and Tantalates. *J. Solid State Chem.* **2006**, *179* (4), 1177–1182.

(13) Myers, L. E.; Eckardt, R. C.; Fejer, M. M.; Byer, R. L.; Bosenberg, W. R.; Pierce, J. W. Quasi-Phase-Matched Optical Parametric Oscillators in Bulk Periodically Poled $LiNbO_3$. *J. Opt. Soc. Am. B* **1995**, *12*, 2102–2016.

(14) Cava, R. J. Dielectric Materials for Applications in Microwave Communications. *J. Mater. Chem.* **2001**, *11*, 54–62.

(15) Cava, R. F.; Peck, W. F.; Krajewski, J. J. Enhancement of the Dielectric Constant of Ta_2O_5 through Substitution with TiO2. *Nature* **1995**, *377* (6546), 215–217.

(16) Robertson, J. High Dielectric Constant Oxides. *Eur. Phys. J. Appl. Phys.* **2004**, *28*, 265-291.

(17) Chaneliere, C.; Autran, J. L.; Devine, R. A. B.; Balland, B. Tantalum Pentoxide (Ta_2O_5) Thin Films for Advanced Dielectric Applications. *Mater. Sci. Eng. R Rep.* **1998**, *22*, 269–322.

(18) Shlyakhtina, A. V.; Belov, D. A.; Pigalskiy, K. S.; Shchegolikhin, A. N.; Kolbanev, I. V.; Karyagina, O. K. Synthesis, Properties and Phase Transitions of Pyrochlore- and Fluorite-like Ln_2RMO_7 (*Ln* = Sm, Ho; *R* = Lu, Sc; *M* = Nb, Ta). *Mater. Res. Bull.* **2014**, *49*, 625–632.

(19) Grey, I. E.; Mumme, W. G.; Roth, R. S. The Crystal Chemistry of L-Ta_2O_5 and Related Structures. *J. Solid State Chem.* **2005**, *178* (11), 3308–3314.

(20) Ferguson, R.B. The Crystallography of Synthetic $YTaO_4$ and Fused Fergusonite. *Can. Mineral.* **1957**, *6*, 72–77.

(21) Kurova, T.A; Aleksandrova, V.B. Crystalline Structure of $LaTaO_4$. *Dokl. Akad. Nauk USSR* **1971**, *201*, 1095–1098.

(22) Markiv, V. Y.; Belyavina, N. .; Markiv, M. .; Titov, Y. .; Sych, A. .; Sokolov, A. .; Kapshuk, A. .; Slobodyanyk, M. . Peculiarities of Polymorphic Transformations in $YbTaO_4$ and Crystal Structure of Its Modifications. *J. Alloys Compd.* **2002**, *346*, 263–268.

(23) Titov, Y. .; Sych, A. .; Sokolov, A. .; Kapshuk, A. .; Markiv, V. Y.; Belyavina, N. . Crystal Structure of the High-Pressure Modification of NdTaO4. *J. Alloys Compd.* **2000**, *311*, 252–255.

(24) Cava, R. J.; Roth, R. S. The Structure of $LaTaO_4$ at 300 °C by Neutron Powder Profile Analysis. *J. Solid State Chem.* **1981**, *36*, 139–147.

(25) Hartenbach, I.; Lissner, F.; Nikelski, T.; Meier, S. F.; Müller-Bunz, H.; Schleid, T. Über Oxotantalate der Lanthanide des Formeltyps $MTaO_4$ (M = La - Nd, Sm - Lu). *Z. Für Anorg. Allg. Chem.* **2005**, *631*, 2377–2382.

(26) Machida, M.; Murakami, S.; Kijima, T.; Matsushima, S.; Arai, M. Photocatalytic Property and Electronic Structure of Lanthanide Tantalates, $LnTaO_4$ (Ln = La, Ce, Pr, Nd, and Sm). *J. Phys. Chem. B* **2001**, *105*, 3289–3294.

(27) Nyman, M.; Rodriguez, M. A.; Rohwer, L. E. S.; Martin, J. E.; Waller, M.; Osterloh, F. E. Unique $LaTaO_4$ Polymorph for Multiple Energy Applications. *Chem. Mater.* **2009**, *21* (19), 731–4737.

(28) Blasse, G.; Dirksen, G. J.; Brixner, L. H.; Crawford, M. K. Luminescence of Materials Based on LuTaO4. *J. Alloys Compd.* **1994**, *209*, 1–6.

(29) Brixner, L. H.; Chen, H. On the Structural and Luminescent Properties of the M′ $LnTaO_4$ Rare Earth Tantalates. *J. Electrochem. Soc.* **1983**, *130*, 2435–2443.

(30) Kolb, E. D.; Laudise, R. A. The Phase Diagram, LiOH-Ta_2O_5-H_2O and the Hydrothermal Synthesis of $LiTaO_3$ and $LiNbO_3$. *J. Cryst. Growth* **1976**, *33*, 145–149.

(31) Mann, M.; Jackson, S.; Kolis, J. Hydrothermal Crystal Growth of the Potassium Niobate and Potassium Tantalate Family of Crystals. *J. Solid State Chem.* **2010**, *183*, 2675–2680.

(32) J. Matthew Mann. *"Hydrothermal Crystal Growth of Tetravalent and Pentavalent Metal Oxides" Ph.D. Thesis, Clemson University*; 2009.

(33) McMillen, C. D.; Kolis, J. W. Bulk Single Crystal Growth from Hydrothermal Solutions. *Philos. Mag.* **2012**, *92*, 2686-2711.

(34) McMillen, C. D.; Kolis, J. W. Hydrothermal Synthesis as a Route to Mineralogically-Inspired Structures. *Dalton Trans.* **2016**, *45*, 2772-2784.

(35) Yokogawa, Y. Order-Disorder in R_3TaO_7 (R = rare Earth) Phases. *Solid State Ion.* **1988**, *28–30*, 1250–1253

(36) Yokogawa, Y.; Yoshimura, M.; Sōmiya, S. Phase Changes and Lattice Distortion in Fluorite-Related Phases of R_3TaO_7 ($3R_2O_3 \cdot Ta_2O_5$, R = Rare Earth). *Mater. Res. Bull.* **1987**, *22*, 1449–1456.

(37) Apex3; Bruker AXS Inc.: Madison, WI, 2015.

(38) Rigaku and Molecular Structure Corporation The Woodlands TX. CrystalClear. **2006**.

(39) Sheldrick, G. M. A Short History of *SHELX*. *Acta Crystallogr. A* **2008**, *64* (1), 112–122.

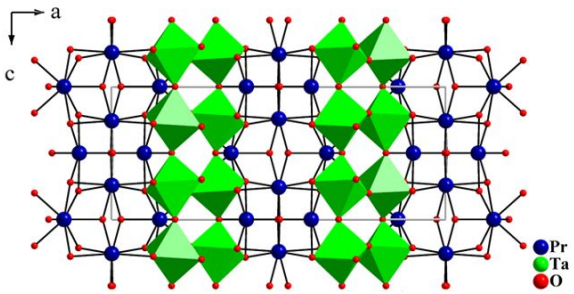

New structure types $Ln_2TaO_5(OH)$ and $Ln_3Ta_2O_9(OH)$ are prepared via hydrothermal synthesis from refractory oxide precursors.